Structure, dynamics, and thermodynamics of ferrofluids

Structure, Dynamics, and Thermodynamics of Ferrofluids

Philip J. Camp

School of Chemistry, University of Edinburgh,

David Brewster Road, Edinburgh EH9 3FJ, Scotland and

Institute of Natural Sciences and Mathematics, Ural Federal University,

51 Lenin Avenue, Ekaterinburg 620000, Russia

(Dated: 29 January 2017)

Abstract

A survey of recent work on the structure, dynamics, and thermodynamics of ferrofluids is given. The emphasis is on new theoretical descriptions and computer simulations of simple models of colloidal ferromagnetic nanoparticles, but some favourable comparisons with experiments are shown to justify the choices of models. The survey summarises combined theoretical and computational studies of field-induced microstructure in ferrofluids, magnetisation curves, static and dynamic initial magnetic susceptibilities, thermodynamic properties, and sedimentation profiles.

I. INTRODUCTION

Ferrofluids contain colloidal magnetic nanoparticles, e.g. of magnetite (Fe_3O_4), stabilised with simple surfactants like oleic acid or oleylamine, and dispersed in a non-magnetic liquid like decalin or kerosene. Ferrofluids are technologically important, finding application as heat-conduction and damping media, liquid sealants, lubricants, and gas-fluidised beds [1]. In biomedicine, water-based magnetic liquids are used in tumour detection and destruction, targeted drug delivery, and magnetic resonance imaging [2, 3]. Ferrofluids are also 'simple' model polar liquids, in which magnetic dipole-dipole and dipole-field interactions play dominant roles [4]. The short-range interactions can be tuned in the normal way with steric stabilisers, and in the case of aqueous ferrofluids, added salt.

At PLMMP 2005 in Kyiv, I had the good fortune of meeting Alexey Ivanov, Ekaterina Elfimova, and Sofia Kantorovich from the Ural Federal University (formerly the Ural State University) in Ekaterinburg, Russia. In the following decade, the Ekaterinburg and Edinburgh teams have developed a broad range of theoretical and simulation techniques to describe ferrofluids, all based on rather simple coarse-grained models (Sect. II). On the theoretical side, new statistical mechanical approaches have been established, such as the modified mean-field theory of the magnetic response, and the logarithmic free-energy theory of the thermodynamic properties. On the simulation side, Monte Carlo and molecular dynamics techniques have been developed to test the theoretical predictions. In this contribution, a selective summary of recent results will be presented, with emphasis on understanding experimental measurements. Examples will include field-induced microstructure (Sect. III), the magnetisation curve (Sect. IV), initial and dynamic magnetic susceptibilities (Sect. V), thermodynamic properties with and without applied fields (Sect. VI), and sedimentation profiles in monodisperse and polydisperse ferrofluids (Section VII).

II. SIMPLE MODELS OF FERROFLUIDS

A schematic diagram of a spherical colloidal ferromagnetic particle is shown in Fig. 1. The magnetic core diameter is x, and assuming that the particle is homogeneously magnetised, the magnetic dipole moment is $\mu = \pi M_{\rm s} x^3/6$ where $M_{\rm s}$ is the saturation magnetisation, usually taken to be the bulk value. The particle is sterically stabilised with a layer of

surfactant molecules of thickness δ, such that the effective particle diameter is $\sigma = x + 2\delta$. The particles are immersed in a simple liquid characterised by regular parameters such as the density and the viscosity η. For small single-domain ferromagnetic particles, the dipole moment has two equally probable orientations in opposite directions along the magnetisation easy axis, and the associated switching between these two directions is called Néel relaxation. The time scale for this relaxation is $\tau_{\mathrm{N}} = \tau_0 \exp(KV/k_{\mathrm{B}}T)$ where $\tau_0 \sim 10^{-9}$ s, K is the anisotropy constant (a material parameter), and $V = \pi x^3/6$ is the magnetic core volume. For larger particles, τ_{N} exceeds the timescale for Brownian rotation $\tau_{\mathrm{B}} = 3V\eta/k_{\mathrm{B}}T$, and so the dipole moment changes direction mainly by particle rotation. For magnetite in kerosene at room temperature ($T = 293$ K) the crossover between the Néel and Brownian regimes is at about 10 nm, and for 16 nm particles, $\tau_{\mathrm{N}} \sim 1$ s and $\tau_{\mathrm{B}} \sim 10^{-6}$ s [1].

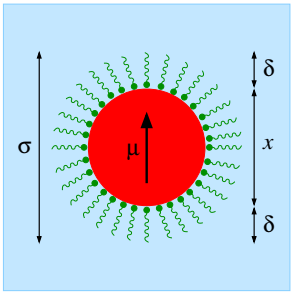

FIG. 1. Schematic diagram of a sterically stabilised ferromagnetic nanoparticle with magnetic core diameter x (shown in red), steric layer thickness δ (shown in green), and effective hard-core diameter $\sigma = x + 2\delta$.

The magnetic field at any point outside of a homogeneously magnetised sphere is identical to that produced by a central point dipole [5], and the magnetic interaction between two such spheres is identical to the interaction between two point dipoles (see Reference [6] for a pedagogical derivation). The magnetic dipole-dipole interaction energy is

$$u_{\mathrm{d}}(\boldsymbol{r}, \boldsymbol{\mu}_i, \boldsymbol{\mu}_j) = \frac{\mu_0}{4\pi}\left[\frac{(\boldsymbol{\mu}_i \cdot \boldsymbol{\mu}_j)}{r^3} - \frac{3(\boldsymbol{\mu}_i \cdot \boldsymbol{r})(\boldsymbol{\mu}_j \cdot \boldsymbol{r})}{r^5}\right] \tag{1}$$

where $\boldsymbol{r}$ is the separation vector, $\boldsymbol{\mu}_i$ is the dipole moment on particle i, and μ_0 is the vacuum magnetic permeability. There are various choices of short-range potential. The simplest choice is the hard-sphere (HS) potential, given by

$$u_{\mathrm{HS}}(r) = \begin{cases} \infty & r < \sigma \\ 0 & r \geq \sigma \end{cases} \tag{2}$$

where $r = |\boldsymbol{r}|$. Another popular choice is the Lennard-Jones (LJ) potential

$$u_{\mathrm{LJ}}(r) = 4\epsilon \left[\left(\frac{\sigma}{r}\right)^{12} - \left(\frac{\sigma}{r}\right)^{6} \right] \tag{3}$$

which contains an attractive component. The combination of the dipolar and LJ potentials is called the Stockmayer model [7]. A convenient, purely repulsive potential for molecular dynamics simulations is the Weeks-Chandler-Andersen (WCA) potential

$$u_{\mathrm{WCA}}(r) = \begin{cases} u_{\mathrm{LJ}}(r) - u_{\mathrm{LJ}}(r_{\mathrm{c}}) & r < 2^{1/6}\sigma \\ 0 & r \geq 2^{1/6}\sigma \end{cases} \tag{4}$$

which is effectively the LJ potential cut and shifted at its minimum. All of these short-range potentials are characterised by the effective particle diameter σ. This allows various physically meaningful parameters to be defined. The dipolar coupling constant is given by

$$\lambda = \frac{\mu_0}{4\pi} \left(\frac{\mu^2}{k_{\mathrm{B}} T \sigma^3} \right) \tag{5}$$

and it characterises the strength of the dipole-dipole interactions as compared to the thermal energy $k_{\mathrm{B}}T$. For magnetite nanoparticles with $x = 10$ nm and $M_{\mathrm{s}} = 4.8 \times 10^5$ A m^{-1}, the dipole moment is $\mu = 2.5 \times 10^{-19}$ A m^2. Assuming a typical value of $\delta = 2$ nm for the thickness of the non-magnetic steric layer (e.g., oleic acid) the hard-core diameter is $\sigma = 14$ nm, and at room temperature ($T = 293$ K) the dipolar coupling constant is $\lambda \simeq 0.6$. The concentration of a ferrofluid is $\rho = N/V$, where N is the number of particles and V is the volume. In reduced units, this is expressed as

$$\rho^* = \rho \sigma^3. \tag{6}$$

A more intuitive measure is the volume fraction, given by

$$\varphi = \frac{\pi \rho^*}{6}. \tag{7}$$

For real ferrofluids, $\varphi \sim 0.1$, although concentrations of up to $\varphi \sim 0.5$ are possible in highly polydisperse samples. Ferrofluids are useful precisely because their properties can be switched with the application of magnetic fields. The strength of the particle-field interaction is measured by the Langevin parameter

$$\alpha = \frac{\mu_0 \mu H}{k_{\mathrm{B}} T} \tag{8}$$

where H is the external magnetic field strength. For the 10 nm magnetite nanoparticles considered above, $\alpha = 1$ corresponds to an external magnetic field $H \simeq 1.3 \times 10^4$ A m^{-1}.

III. FERROFLUID MICROSTRUCTURE

The lowest-energy arrangement of a pair of dipolar spheres is the nose-to-tail parallel ($\rightarrow\rightarrow$) configuration. The ground-state configuration of four or more dipolar spheres is a ring [8]. At low temperatures, chains are common structural motifs because they also have very low energy, but higher entropy than rings. It is also possible to observe branching points, where a particle is connected to three or four near neighbours [9, 10]. All of these structures have been observed in experiment and in simulations. Experimentally, ferrofluid structure can be observed using cryogenic transmission electron microscopy [11–14]. In simulations at low temperature ($\lambda \geq 4$) chains are dominant at moderate concentrations [15–17], while rings are the most common structural motif at very low concentrations [18]. At higher concentrations, clusters give way to 'normal' dense-liquid structures. It is also thought that spontaneously magnetised fluid domains can form at low temperatures and high concentrations [19–24].

Ferrofluids undergo field-induced structuring, with chain-like clusters aligning and growing in the field direction. In recent work, the growth of chain-like orientational correlations was studied using theory and Monte Carlo computer simulations [25, 26]. The theoretical approach is based on a virial expansion of the pair distribution function

$$g(r,\theta) = \sum_{k=0}^{\infty}\sum_{l=0}^{\infty} \varphi^k \lambda^l \beta_{kl}(r,\theta) \tag{9}$$

where the coefficients β_{kl} are functions of the interparticle separation r, and the angle of the separation vector $\boldsymbol{r}$ with the applied magnetic field $\boldsymbol{H}$, i.e., $\boldsymbol{r}\cdot\boldsymbol{H} = rH\cos\theta$. Fig. 2(a) and (c) shows typical results for $g(r,\theta)$ in a monodisperse fluid of dipolar hard spheres with $\lambda = 1$, $\varphi = 0.1$, and $\alpha = 0$ and 5 [25]. ($\alpha = 5$ corresponds to a ferrofluid magnetisation of about 80% of the saturation value – see Sect. IV.) Note that $g(r,\theta) = 0$ for $r < \sigma$. The theoretical curves correspond to a truncation of Eq. 9, keeping only the terms β_{00} (the hard-sphere pair distribution function from Percus-Yevick theory [27]), β_{01}, β_{02}, β_{11}, and β_{12}. Hence, only terms of orders up to φ and λ^2 are retained. The truncation in φ means that only the effects of a third particle on the pair distribution function are considered. The results show the growth in positional correlations in the direction parallel to the field (chain-like ordering) while in the perpendicular direction, there is a decrease in structure due to there being no lateral ordering of chain-like clusters. In neutron-scattering experiments it is possible to

detect field-induced ordering by measuring the structure factor $S(\boldsymbol{k})$ at wavevectors $\boldsymbol{k}$ both parallel and perpendicular to the field direction [28–32]. $g(r,\theta)$ and $S(\boldsymbol{k})$ are related by a Fourier transform, and Fig. 2(b) and (d) shows comparisons of the structure factor of the same ferrofluid from theory and simulation. Since the theory is truncated at the three-body level, correlations beyond $r \geq 2\sigma$ will not be described very accurately, and hence the theoretical structure factor will be inaccurate for $k\sigma \leq \pi$. These portions of $S(k)$ are shown as dashed lines. This limitation notwithstanding, the increase in structure parallel to the field, and the decrease in structure perpendicular to the field, are described quite faithfully in the region of the primary peak ($k\sigma \simeq 2\pi$) by the simple virial expansion. This type of analysis has also been applied to the more complex situation of a bidisperse ferrofluid, in describing all of the pair distribution functions and structure factors connecting small and large dipolar particles [26].

IV. MAGNETISATION CURVE

The magnetisation curve $M(H)$ is a very important property of a ferrofluid. Associated with that is the initial susceptibility, which will be considered separately in Sect. V. The magnetisation curves of condensed matter have been studied for more than 100 years, beginning with Langevin's theory of non-interacting particles [33] which gives

$$M_{\mathrm{L}}(H) = \left(\frac{N\mu}{V}\right)\left(\coth\alpha - \frac{1}{\alpha}\right). \tag{10}$$

As mentioned above in Sect. III, when $\alpha = 5$, $M_{\mathrm{L}}(H) \simeq 0.8N\mu/V$. For real ferrofluids, the non-interacting particle picture is inaccurate, particularly in weak fields, where the particle-particle interactions are at least as important as the particle-field interactions. There are many schemes for taking account of the interparticle interactions, including Weiss mean-field theory [34, 35], integral equations [36, 37], thermodynamic perturbation theory [38, 39], so-called modified mean-field theories [40, 41], Mayer cluster expansions [42–44], and density functional theory [45–47]. One of the most successful theories is the second-order modified mean-field (MMF2) theory, which is based on an expansion of the pair correlation function in terms of φ and λ, and its connection through the Yvon-Born-Green hierarchy [27] with the one-particle density, from which the magnetisation can be computed. The key result is that the magnetisation curve can be expressed by a Langevin-type expression but with an

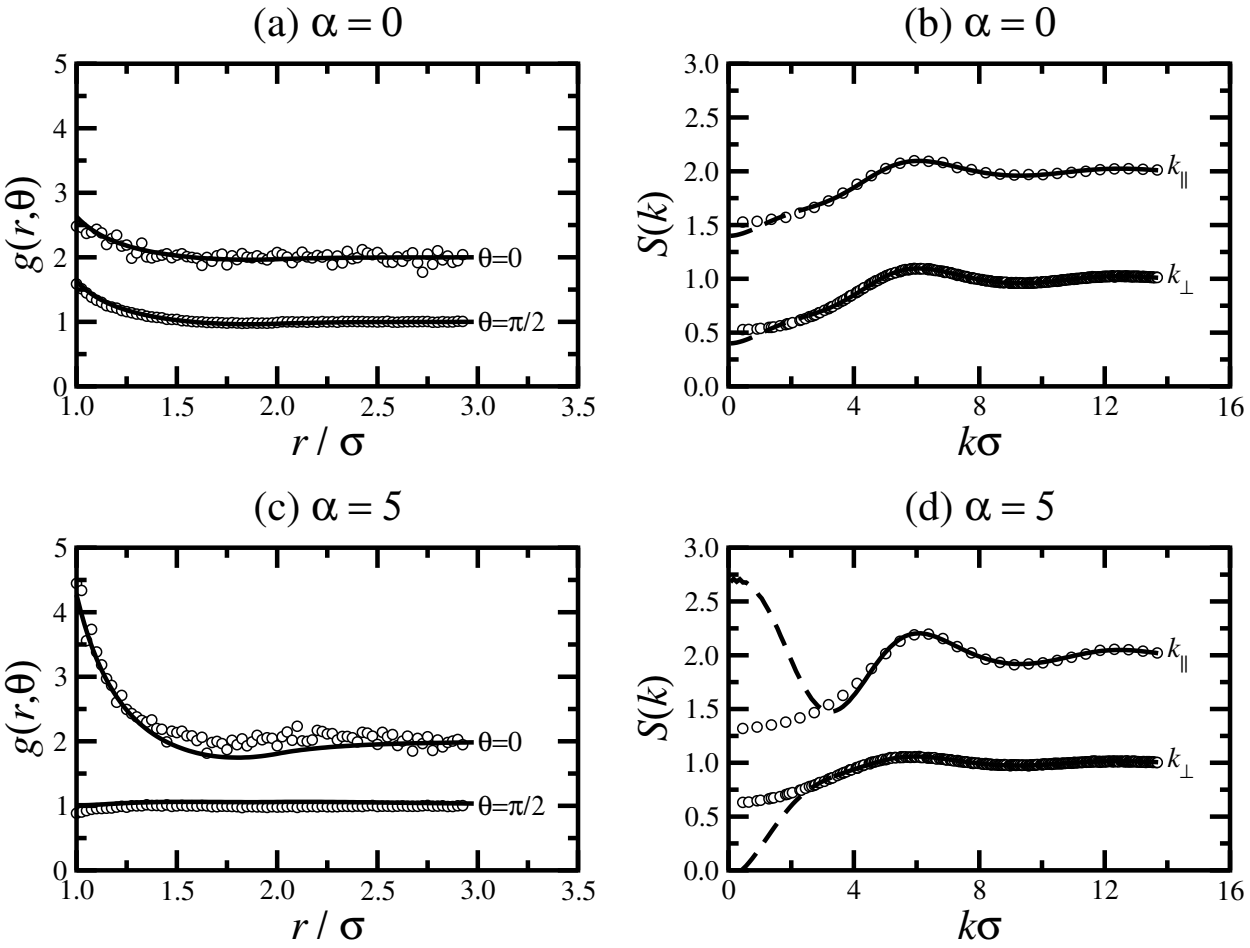

FIG. 2. Pair distribution function $g(r,\theta)$ [(a) and (c)] and structure factor $S(\boldsymbol{k})$ [(b) and (d)] for a monodisperse fluid of dipolar hard spheres with $\lambda = 1$, $\varphi = 0.1$, and $\alpha = 0$ [(a) and (b)] and 5 [(c) and (d)]. The results for $\theta = 0$ and $k_{\|}$ are shifted up by one unit for clarity.

effective field $H_{\rm eff}$ modified by the contributions from the other particles.

$$M(H) = M_{\rm L}(H_{\rm eff}) \tag{11}$$

The effective field is of course given by an expansion, which at the MMF2 level is

$$H_{\rm eff} = H + \frac{1}{3}M_{\rm L}(H) + \frac{1}{144}M_{\rm L}(H)\frac{{\rm d}M_{\rm L}(H)}{{\rm d}H} + \ldots \tag{12}$$

The MMF2 has been tested critically against both experimental and simulation data for polydisperse ferrofluids [48, 49]. The particle-size distribution $p(x)$ is generally unknown, but the accuracy of the theory can be assessed by fitting the distribution to experimental data, and then checking the theory against essentially exact simulations with the fitted particle-size

distribution. Crucially, experimental data are available for ferrofluids prepared at various concentrations by dilution of the same high-concentration stock suspension. This means that, at the very least, an accurate theory should give the same particle-size distribution at each concentration. The particle-size distribution is conveniently expressed in terms of a Γ-distribution with only two parameters, a and x_0:

$$p(x) = \frac{x^a \exp\left(-x/x_0\right)}{x_0^{a+1}\Gamma(a+1)}. \tag{13}$$

Interestingly, of all of the approaches mentioned above, only the MMF2 theory gives the same fitted parameters over all concentrations. For the particular ferrofluid under consideration [48, 49], $a = 4.95$ and $x_0 = 1.23$ nm, with a mean magnetic-core diameter of $(a+1)x_0 = 7.32$ nm, and polydispersity $\sqrt{\langle x^2\rangle - \langle x\rangle^2)}/\langle x\rangle = 0.41$. The quality of the fits is illustrated in Fig. 3, which shows $M(H)$ for ferrofluid samples with saturation magnetisations $M(\infty) =$ 5.0, 7.8, 11.2, 16.9, 25.3, 37.8, and 57.0 kA m^{-1} (in order of increasing particle concentration). The agreement between theory, experiment, and simulation is excellent in all cases, and over the full range of magnetic field.

V. MAGNETIC SUSCEPTIBILITY

A. Static susceptibility

The initial magnetic susceptibility is an important material parameter, and is defined by

$$\chi = \left(\frac{\partial M}{\partial H}\right)_{H=0}. \tag{14}$$

The Langevin susceptibility $\chi_{\rm L}$ is easily determined from the corresponding magnetisation curve in Eq. 10:

$$\chi_{\rm L} = \frac{N\mu_0\mu^2}{3Vk_{\rm B}T} = \frac{4\pi\rho^*\lambda}{3} = 8\varphi\lambda. \tag{15}$$

As with the magnetisation curve, this is going to be a very poor approximation for any real ferrofluid. The MMF theories provide a framework for introducing interparticle interactions. At the MMF2 level, the expression for the initial susceptibility is [41]

$$\chi = \chi_{\rm L}\left(1 + \frac{1}{3}\chi_{\rm L} + \frac{1}{144}\chi_{\rm L}^2\right) \tag{16}$$

while at the MMF1 level, the last term in brackets is omitted. Since $\chi_{\rm L} \propto \varphi\lambda$, it is clear that the MMF theories correspond to retaining only those terms of order $\varphi\lambda$, $(\varphi\lambda)^2$, and

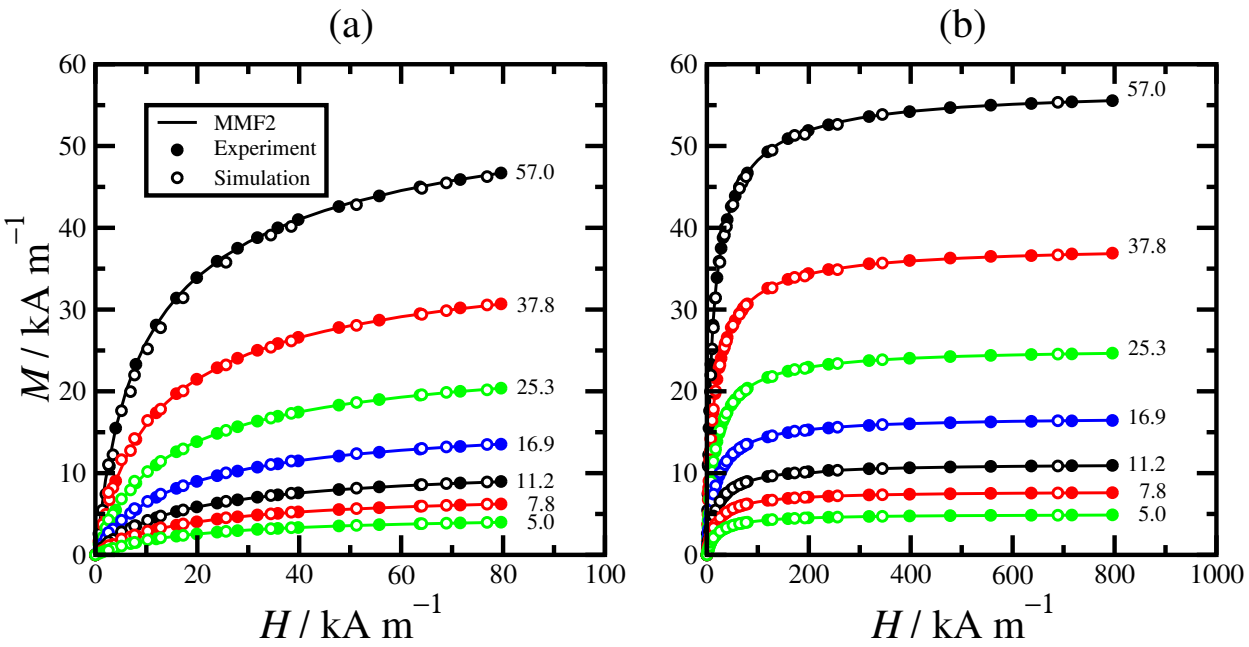

FIG. 3. Magnetisation curves for a polydisperse ferrofluid from theory (lines), experiment (filled points), and simulation (unfilled points): (a) low-field behaviour $H = 0$–80 kA m^{-1}; (b) full magnetisation curve $H = 0$–800 kA m^{-1}. The curves are labelled with the saturation magnetisation $M(\infty)$ in units of kA m^{-1}.

$(\varphi\lambda)^3$. In principle, additional terms of different orders should be included. For example, the first correction to the MMF1-level term gives

$$\chi = \chi_{\mathrm{L}}\left[1 + \frac{1}{3}\chi_{\mathrm{L}}\left(1 + \frac{A}{25}\lambda^2\right) + \frac{1}{144}\chi_{\mathrm{L}}^2\right] \tag{17}$$

where A is a parameter depending only on the short-range potential and the temperature. For hard spheres, $A = 1$, while for the WCA potential at a temperature $k_{\mathrm{B}}T/\epsilon = 1$, $A = 0.943$ [41]. Eq. 17 now contains terms of order $\varphi^2\lambda^4$, and hence will be referred to as MMF2$+\varphi^2\lambda^4$. Fig. 4(a) shows the magnetic susceptibility of a monodisperse fluid of dipolar WCA particles at temperature $k_{\mathrm{B}}T/\epsilon = 1$ [50]. The points are from Brownian dynamics simulations under two sets of conditions: $\lambda = 1$ and at various concentrations; and $\varphi = 0.105$ and with various dipolar coupling constants. The data are shown on the same scale by plotting χ as a function of the Langevin susceptibility χ_{L} given in Eq. 15. Several theoretical curves are shown: the Langevin model; the MMF1 theory; the MMF2 theory; the MMF2$+\varphi^2\lambda^4$ theory at fixed $\lambda = 1$; and the MMF2$+\varphi^2\lambda^4$ theory with $\lambda = \chi_{\mathrm{L}}/8\varphi$ and $\varphi = 0.105$. The results show that the MMF1 theory and the MMF2 theory are very similar,

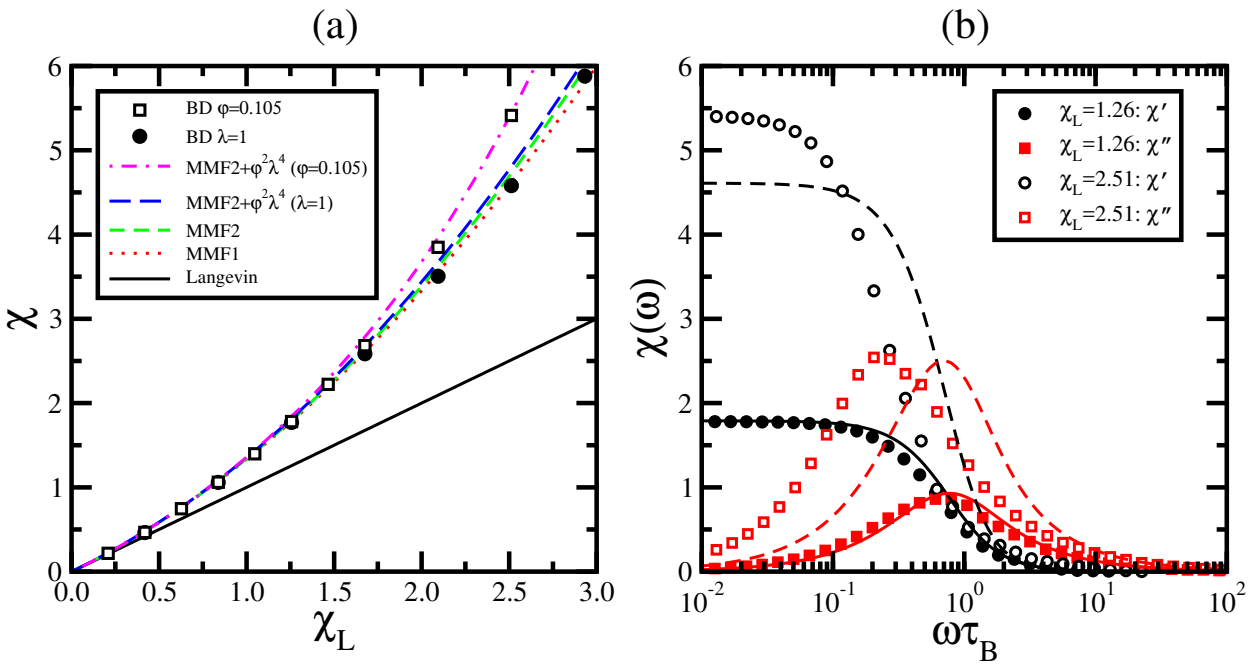

FIG. 4. (a) Initial magnetic susceptibility χ for a monodisperse fluid of dipolar WCA particles at $k_{\rm B}T/\epsilon = 1$. The filled circles and unfilled squares are from Brownian dynamics simulations with $\lambda = 1$ (and various concentrations) and at $\varphi = 0.105$ (with various dipolar coupling constants), respectively. The lines represent various theories – see text. (b) Magnetic susceptibility spectra $\chi(\omega)$ for dipolar WCA particles at $\varphi = 0.105$ and with $\lambda = 1.5$ ($\chi_{\rm L} = 1.26$) (filled points and solid lines), and at $\varphi = 0.105$ and with $\lambda = 3.0$ ($\chi_{\rm L} = 2.51$) (unfilled points and dashed lines). The real and imaginary parts from simulations are shown as black circles and red squares, respectively, and the corresponding theoretical predictions are shown in black and red lines, respectively.

and in good agreement with the simulation results with $\lambda = 1$ over the whole range of $\chi_{\rm L}$ and hence φ. The MMF1 and MMF2 theories are not as accurate with $\varphi = 0.105$ and with large values of λ, but by including the extra term of order $\varphi^2\lambda^4$ in Eq. 17, the agreement is greatly improved. These theories have been applied successfully to the description of real polydisperse ferrofluids [48, 49, 51], and extended to treat dense materials with record-breaking initial susceptibilities approaching 100 [52, 53]. An unusual situation occurs in low-concentration ferrofluids at very low temperature, where ring formation leads to flux closure and hence a dramatic drop in χ; this situation can be described using a cluster model [54].

A few comments are in order to put the current results in to context with well-known

results for electrically polar liquids [27, 55]. The electrical analogue of the static susceptibility χ is $(\varepsilon - 1)$, where ε is the static dielectric constant. The dielectric constant of a spherical sample surrounded by a continuum with dielectric constant ε' is given by [56, 57]

$$\frac{(\varepsilon - 1)(2\varepsilon' + 1)}{(\varepsilon + 2\varepsilon')} = 3yg_{\mathrm{K}} \tag{18}$$

where $y = \rho\mu^2/9\varepsilon_0 k_{\mathrm{B}}T$, ε_0 is the vacuum permittivity, and $g_{\mathrm{K}} = \langle M^2\rangle/N\mu^2$ is the Kirkwood factor. g_{K} is determined by the correlations between particles, and is equal to

$$g_{\mathrm{K}} = 1 + \int \mathrm{d}\boldsymbol{r} \int \mathrm{d}\boldsymbol{e}_1 \int \mathrm{d}\boldsymbol{e}_2 h(\boldsymbol{r}, \boldsymbol{e}_1, \boldsymbol{e}_2)(\boldsymbol{e}_1 \cdot \boldsymbol{e}_2) \tag{19}$$

where $\boldsymbol{\mu}_i = \mu\boldsymbol{e}_i$, $\boldsymbol{e}_i$ is the unit orientation vector for particle i, and $h(\boldsymbol{r}, \boldsymbol{e}_1, \boldsymbol{e}_2)$ is the pair correlation function. The dielectric constant should not depend on the sample geometry and surroundings, which implies that both g_{K} and h depend on sample details [27]. It is interesting to note the various predictions of Eq. 18 in the absence of any orientational correlations between particles ($g_{\mathrm{K}} = 1$), and with the magnetic equivalent of y being $\frac{1}{3}\chi_{\mathrm{L}}$. If $\varepsilon' = 1$ (vacuum surroundings) then Eq. 18 gives, in the magnetic picture, $\chi/(\chi + 3) = \frac{1}{3}\chi_{\mathrm{L}}$, and hence $\chi = \chi_{\mathrm{L}}/(1 - \frac{1}{3}\chi_{\mathrm{L}}) = \chi_{\mathrm{L}}(1 + \frac{1}{3}\chi_{\mathrm{L}} + \frac{1}{9}\chi_{\mathrm{L}}^2 + \ldots)$. The first and second terms in brackets are exact, while the third is merely of the correct sign. This is the Weiss (or Debye) mean-field model in which the effective field experienced by the particles is $H_{\mathrm{eff}} = H + \frac{1}{3}M$, with M determined self-consistently from the Langevin formula (11) [34, 35]. The theory also predicts a divergence in χ at $\chi_{\mathrm{L}} = 3$, signalling a spontaneous transition to a ferromagnetic state which has not been observed experimentally. In the Onsager-Kirkwood model $\varepsilon' = \varepsilon$ [58, 59] and hence the magnetic equivalent is $\chi(2\chi + 3)/(\chi + 1) = 3\chi_{\mathrm{L}}$. This gives for the susceptibility $\chi = \chi_{\mathrm{L}}(1 + \frac{1}{3}\chi_{\mathrm{L}}^2 - \frac{1}{9}\chi_{\mathrm{L}}^2 + \ldots)$; the third term in the brackets is of the wrong sign [60]. Finally, when $\varepsilon' = \infty$, the result is simply $\chi = \chi_{\mathrm{L}}$. Nonetheless, this last case provides the most convenient expression for χ given the appropriate virial expansion of h and hence g_{K} [61–64], and it also corresponds directly to the conducting boundary conditions that are most often used in computer simulations. This discussion shows that there are many ways to approach the calculation of χ, and that the results are often complicated and substantially different for a given level of approximation. The conclusion is that the MMF2 approach – and extensions of it – provides a convenient and accurate means of describing the static susceptibility of real ferrofluids based only on knowledge of χ_{L}.

B. Dynamic susceptibility

The dynamic initial magnetic susceptibility – or magnetic susceptibility spectrum $\chi(\omega)$ – is important for determining the dissipation of heat in ferrofluids subject to AC magnetic fields. The power dissipation is proportional to the square of the imaginary (or out-of-phase) part of the spectrum, $\chi''(\omega)$ [65]. This physical effect is utilised in hyperthermia treatments of tumours [2, 3, 66–68]. In the Brownian relaxation regime (as opposed to the Néel relaxation regime described in Sect. II) the orientational dynamics of a single isolated dipolar particle are described by the Fokker-Planck equation [69, 70]

$$\frac{1}{D_\mathrm{r}}\frac{\partial W}{\partial t} = \frac{1}{\sin\theta}\frac{\partial}{\partial\theta}\left[\sin\theta\left(\frac{\partial W}{\partial\theta} + \frac{W}{k_\mathrm{B}T}\frac{\partial U}{\partial\theta}\right)\right] \tag{20}$$

where $D_\mathrm{r} = k_\mathrm{B}T/\pi\eta\sigma^3$ is the rotational diffusion coefficient, $W(\theta, t)$ is the one-particle probability density of the orientation of the dipole moment, and θ is the angle between the dipole moment and the applied AC field. The dipole-field interaction energy is

$$\frac{U}{k_\mathrm{B}T} = -\frac{\mu_0[\boldsymbol{\mu}\cdot\boldsymbol{H}(t)]}{k_\mathrm{B}T} = -\alpha(\cos\theta)e^{-i\omega t}. \tag{21}$$

The Fokker-Planck equation is easily solved in the weak-field case ($\alpha \to 0$, corresponding to the initial or linear-response regime) to give W, from which the magnetisation response $\boldsymbol{M}(t)$ can be determined. The proportionality between $\boldsymbol{M}(t)$ and $\boldsymbol{H}(t)$ is the frequency-dependent initial susceptibility $\chi(\omega)$. For a single isolated particle, the real part $[\chi'(\omega)]$ and imaginary part $[\chi''(\omega)]$ are given by the familiar Debye expressions

$$\chi'_\mathrm{D}(\omega) = \frac{\chi_\mathrm{L}}{1+(\omega\tau_\mathrm{B})^2} \tag{22}$$

$$\chi''_\mathrm{D}(\omega) = \frac{\chi_\mathrm{L}\omega\tau_\mathrm{B}}{1+(\omega\tau_\mathrm{B})^2} \tag{23}$$

where $\tau_\mathrm{B} = 1/2D_\mathrm{r}$ is the Brownian rotation time. To take account of interactions between particles, a similar approach to that outlined in Sect. IV is taken. The effective magnetic field felt by a single particle is the sum of the applied external field and the contribution from all of the other particles. At the MMF1 level, this effective field gives an interaction energy equal to [71]

$$\frac{U}{k_\mathrm{B}T} = -\frac{\mu_0[\boldsymbol{\mu}\cdot\boldsymbol{H}_\mathrm{eff}(t)]}{k_\mathrm{B}T} = -\alpha(\cos\theta)e^{-i\omega t}\left[1+\frac{1}{3}\chi_\mathrm{D}(\omega)\right]. \tag{24}$$

Substituting this interaction energy in to the Fokker-Planck equation gives the result

$$\chi'(\omega) = \chi'_{\rm D}(\omega) + \frac{1}{3}\left\{[\chi'_{\rm D}(\omega)]^2 - [\chi''_{\rm D}(\omega)]^2\right\} \tag{25}$$

$$\chi''(\omega) = \chi''_{\rm D}(\omega)\left[1 + \frac{2}{3}\chi'_{\rm D}(\omega)\right]. \tag{26}$$

Fig. 4(b) shows magnetic susceptibility spectra for dipolar WCA particles at $k_{\rm B}T/\epsilon = 1$ and fixed concentration $\varphi = 0.105$, from Brownian dynamics simulations and the dynamical MMF1 theory [50, 72]. Two sets of data are shown: one with $\lambda = 1.5$ (or $\chi_{\rm L} = 1.26$) which is in the regime where the MMF1-level theory for the zero-frequency susceptibility $\chi'(0)$ is accurate; and the other with $\lambda = 3.0$ (or $\chi_{\rm L} = 2.51$) which is beyond the regime where MMF1 theory is expected to work. Firstly, the simulation results show that the peak frequency decreases with increasing dipolar interaction strength. This is due to the growth of chain-like correlations between particles, and the associated 'slowing down' of the rotational motion of small clusters. Secondly, the simulation results with $\chi_{\rm L} = 1.26$ are rather well described by the dynamical MMF1 theory, which gets right both the zero-frequency susceptibility $\chi'(0)$ and the position of the peak in $\chi''(\omega)$. Finally, there are substantial deviations between simulation and theory in the strong-interaction case ($\chi_{\rm L} = 2.51$) due to the truncation of the effective-field term in Eq. 24. In principle, there should be additional terms akin to those in Eq. 12 and Eq. 17. This is an ongoing problem. As tested against experimental data for real, polydisperse ferrofluids, the dynamical MMF1 theory does rather well [71, 73].

VI. THERMODYNAMIC FUNCTIONS

A. Free energy and equation of state

The thermodynamic properties of colloidal suspensions are of huge interest and importance. Central to all equilibrium thermodynamics is the Helmholtz free energy F. If F is known as a function of concentration and temperature, then all other thermodynamic functions can be determined using standard relations. It can also be used to examine inhomogeneous systems, within the bounds of the local-density approximation: see Sect. VII for examples. There are many ways of estimating F, but a recently proposed route has proven to be particularly simple and effective – the so-called logarithmic free-energy theory. The

standard virial expansion of F is [27]

$$F = F_{\rm id} + Nk_{\rm B}T\sum_{n=1}^{\infty}\frac{1}{n}B_{n+1}\varphi^n \tag{27}$$

where B_n is the $n^{\rm th}$ virial coefficient. For dipolar particles, and accounting for the possibility of applying an external magnetic field, the expressions for the second and third virial coefficients are as follows [74].

$$B_2 = -\frac{1}{2}\int {\rm d}\boldsymbol{r}_{12}\langle f_{12}\rangle \tag{28}$$

$$B_3 = -\frac{1}{3}\int {\rm d}\boldsymbol{r}_{12}\int {\rm d}\boldsymbol{r}_{13}\langle f_{12}f_{23}f_{13}\rangle + \int {\rm d}\boldsymbol{r}_{12}\int {\rm d}\boldsymbol{r}_{13}\left[\langle f_{12}\rangle\langle f_{13}\rangle - \langle f_{12}f_{13}\rangle\right] \tag{29}$$

$f_{ij} = [\exp\left(-u_{ij}/k_{\rm B}T\right)-1]$ is the Mayer f-function between particles i and j, where u_{ij} is the total pair potential. The angled brackets denote an orientational average weighted by the Boltzmann factor involving the particle-field interaction energies for each of the particles, e.g.,

$$\langle f_{12}\rangle = \left(\frac{\alpha}{4\pi\sinh\alpha}\right)^2\int {\rm d}\boldsymbol{e}_1\int {\rm d}\boldsymbol{e}_2 f_{12}\exp\left(\alpha\cos\theta_1 + \alpha\cos\theta_2\right) \tag{30}$$

where θ is the angle between $\boldsymbol{e}$ and the applied field. The expression for B_2 is standard, but the expression for B_3 contains an extra (second) term which is not often included in textbook derivations. If the external field is zero or infinity (meaning $\alpha = 0, \infty$) then the 'fluctuation' term in square brackets disappears. But for all other finite field strengths, this term is non-zero, and typically represents about 10% of the total value of B_3. From the theoretical point of view, the calculation of virial coefficients is arduous. In the case of dipolar particles in zero field, it is possible to determine B_2 and B_3 rather accurately as expansions in powers of λ, up to about $\lambda \simeq 4$ [75]. In the presence of a field, these expansions involve additional complicated functions of α, and the range is currently limited to $\lambda \leq 2$. The validity and range of application of these expansions have been tested using numerical data from Mayer-sampling Monte Carlo calculations [74, 75].

The virial expansion is slow to converge, if at all. Given that higher order virial coefficients are rarely available, one way of extending the virial-expansion approach is to write a so-called perturbed virial expansion in the form

$$F = F_{\rm ref} + Nk_{\rm B}T\sum_{n=1}^{\infty}\frac{1}{n}\Delta B_{n+1}\varphi^n \tag{31}$$

where F_{ref} is the free energy of a well-characterised reference system such as the hard-sphere fluid, and ΔB_n is the difference in virial coefficients between the system of interest and the reference system. This follows closely an idea by Nezbeda and co-workers who wrote a similar expression for the pressure [76–78]. Going one step further, remembering that F is proportional to the logarithm of the partition function, the logarithm can be 'put back in' by writing [74, 75]

$$F = F_{\text{ref}} - Nk_{\text{B}}T \ln\left(1 + \sum_{n=1}^{\infty} \frac{1}{n} I_{n+1} \varphi^n\right) \tag{32}$$

where the coefficients I_n must reproduce the perturbed virial expansion as a Maclaurin series in φ. The first two coefficients are $I_2 = -\Delta B_2$ and $I_3 = -\Delta B_3 + \Delta B_2^2$. The benefit of this logarithmic free-energy expression is that an expansion of the logarithm generates terms of all orders in φ, and so higher-order terms in the virial expansion are generated, albeit approximately. For the dipolar hard-sphere model, Eqs. 27, 31, and 32 have been tested critically against the results of Monte Carlo simulations [75]. Fig. 5(a) shows a comparison between the simulation results and the predictions of the virial expansion and the logarithmic free-energy theory with B_2, B_3, and B_4 represented as polynomial expansions. Results are shown over a broad range of concentration $0 \leq \varphi \leq 0.5$, and with dipolar coupling constants $\lambda = 1$–4. With $\lambda = 1$–3, the logarithmic free-energy theory is in excellent agreement with simulation results. The original virial expansion is only accurate at very low concentrations. With $\lambda = 4$, neither of the theories is particularly good, although this is at the onset of the chaining regime (see Sect. III) and so any theory limited to two-, three-, or four-particle correlations is always going to struggle. The same methodology can be applied to systems in the presence of a field. Fig. 5(b) shows the compressibility factor $PV/Nk_{\text{B}}T$, with the pressure given by $P = -(\partial F/\partial V)_T$. The predictions of the perturbed virial expansion and the logarithmic free-energy theory are compared to the results from Monte Carlo simulations with $\lambda = 1$ and $\alpha = 5$ [74]. The same expressions for the second and third virial coefficients are used in the two theories. The agreement with simulation clearly shows the substantial benefit of the logarithmic formulation.

The logarithmic free-energy approach has been applied successfully to osmotic equations of state measured in ultracentrifugation experiments [75, 79, 80] and to the Stockmayer fluid [81]. Since the virial coefficients and the free energy are known as functions of the applied field, it is possible to determine the magnetisation curves, although the approach is not as

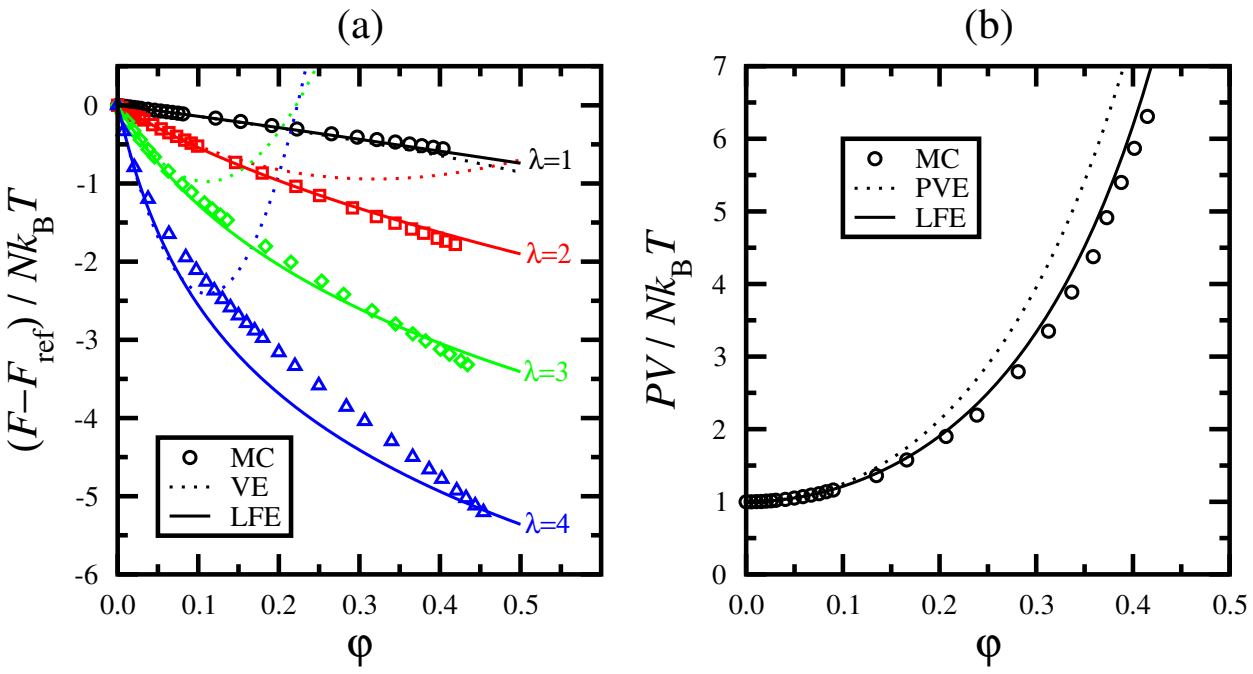

FIG. 5. (a) The difference in Helmholtz free energy between that of the dipolar hard-sphere model with dipolar coupling constant λ and that of the hard-sphere model ($\lambda = 0$). The points are from Monte Carlo simulations (MC), the dotted lines are from the original virial expansion (VE), and the solid lines are from the logarithmic free-energy theory (LFE). (b) The compressibility factor PV/Nk_BT for the dipolar hard-sphere model in an applied field, with $\lambda = 1$ and $\alpha = 5$. The points are from Monte Carlo simulations (MC), the dotted line is from the perturbed virial expansion (PVE), and the solid line is from the logarithmic free-energy theory (LFE).

good as the MMF2 theory [74]. The thermodynamic theory has also been used to great effect in the analysis of sedimentation profiles; this is discussed in Sect. VII.

B. Phase diagram

The phase diagram of strongly interacting dipolar particles is a vast topic in its own right. In 1970 de Gennes and Pincus predicted that the phase diagram of purely dipolar particles (with no additional attractive interactions) would be very similar to that of a simple atomic fluid [82]. The argument put forward was that the leading-order term in the orientationally averaged potential of mean force is attractive and proportional to $1/r^6$. In combination with a simple short-range repulsive interaction, this would indeed give rise to

distinct liquid and vapour phases. A more detailed analysis suggests that the vapour-liquid critical point should belong to the Ising universality class [83]. All standard approaches to the vapour-liquid transition – thermodynamic perturbation theory, integral equations, logarithmic free-energy theory, etc. – predict a vapour-liquid critical point in the region of $\lambda = 3$–4. As discussed in Sect. III, this is roughly where particle clustering begins. It appears from computer simulations that cluster formation does indeed interfere with phase separation, either through chaining [84, 85] or ring formation [86]. In either scenario, computer simulations are somewhat limited, in that the system sizes currently accessible are not very large as compared to the likely density-density correlation lengths between clusters. If there were a condensation transition of chains or rings driven by weak cluster-cluster interactions, then simulations of relatively small systems would not be able to accommodate the density fluctuations associated with a nearby critical point. From the practical point of view, a transition can be brought in to existence with very small perturbations to the system, e.g., contributions from higher multipole moments [87], added non-polar particles [88], and very weak additional isotropic interactions [89–91]. To sum up, on the basis of computer simulation results, it would appear that there is no vapour-liquid phase transition driven purely by dipolar interactions. Theories can always be constructed that mirror the current simulation results [9, 92, 93], but it remains an open theoretical challenge to prove that a dipole-driven transition does not exist, or if it does exist, then to predict under what physical conditions it can be observed.

VII. SEDIMENTATION

In this final section, the influence of thermodynamics on structure will be examined in the context of sedimentation profiles. Under certain conditions that are usually met in normal colloidal suspensions [94–96], analytical (ultra)centrifugation experiments provide a direct link between the concentration profile and the osmotic equation of state, and hence the thermodynamics. As mentioned in Sect. VI, such experiments on ferrofluids have provided equations of state that could be compared directly with theory and simulation [79, 80]. The key relation linking the gradient diffusion and sedimentation of particles in suspension is

$$-G = \frac{1}{k_{\mathrm{B}}T}\left(\frac{\partial\mu}{\partial\varphi}\right)\frac{\mathrm{d}\varphi}{\mathrm{d}z} \tag{33}$$

where G^{-1} is the usual gravitational length (a function of the particle size, the particle and liquid mass densities, and the temperature), z is in the direction of increasing gravitational potential, and $\mu = (\partial F/\partial N)$ is the chemical potential (not to be confused with the dipole moment). This expression – corresponding to the local-density approximation – is only reliable if the gravitational length is large compared to the particle size, so that particle layering is absent. From the theoretical standpoint, the chemical potential can be obtained from the logarithmic free-energy theory from Sect. VI, and then Eq. 33 can be integrated to yield the concentration profile $\varphi(z)$. Experimentally, the concentration profile in ferrofluids can be measured using either the optical transmission [79, 80] or the local susceptibility [97]; in the latter case, $\varphi(z)$ can be obtained from $\chi(z)$ using a relation such as Eq. 16.

In recent work, the theoretical approach was validated against precise Monte Carlo simulation results, and applied to the analysis of experimental measurements [98]. Fig. 6(a) shows a comparison of concentration profiles in a bidisperse ferrofluid consisting of a mixture of 'small' (s) particles with diameter σ_s, dipolar coupling constant $\lambda_\mathrm{s} = 1$, and gravitational length $G_\mathrm{s}^{-1} = 20\sigma_\mathrm{s}$, and 'large' (l) particles with $\sigma_\mathrm{l} = 1.25\sigma_\mathrm{s}$, $\lambda_\mathrm{l} = 1.95$, and $G_\mathrm{l}^{-1} = 10.2\sigma_\mathrm{s}$. The surface concentrations were $n_\mathrm{s}\sigma_\mathrm{s}^2 = 13.4$ and $n_\mathrm{l}\sigma_\mathrm{s}^2 = 2.9$, respectively. Eq. 33 can easily be extended to mixtures of particles, and using a suitably generalised logarithmic free-energy theory with B_2 and B_3 as inputs, the predicted concentration profiles are in excellent agreement with those measured in simulations. Fig. 6(b) shows the initial magnetic susceptibility profile for a real polydisperse ferrofluid, along with best fits with either a monodisperse or bidisperse model for the fluid. The fit parameters are the magnetic-core diameters and the relative concentrations of small and large particles; the overall content of magnetic material is fixed. The link between $\varphi(z)$ and $\chi(z)$ is made at the MMF2 level. It is easy to explain why the bidisperse model gives the correct sharp rise in $\chi(z)$ near the bottom of the profile. Fig. 6(a) shows that large particles are localised near the bottom of the sample, and the large particles have larger susceptibility by virtue of the larger dipole moment. Hence, the total susceptibility profile in a bidisperse system shows a sharper drop with increasing height than does a monodisperse system. In general, it is rather difficult to determine the particle-size distribution $p(x)$ without making some assumptions about the precise mathematical form, but even a two-component model is sufficient to capture the major effects of polydispersity [26, 99, 100].

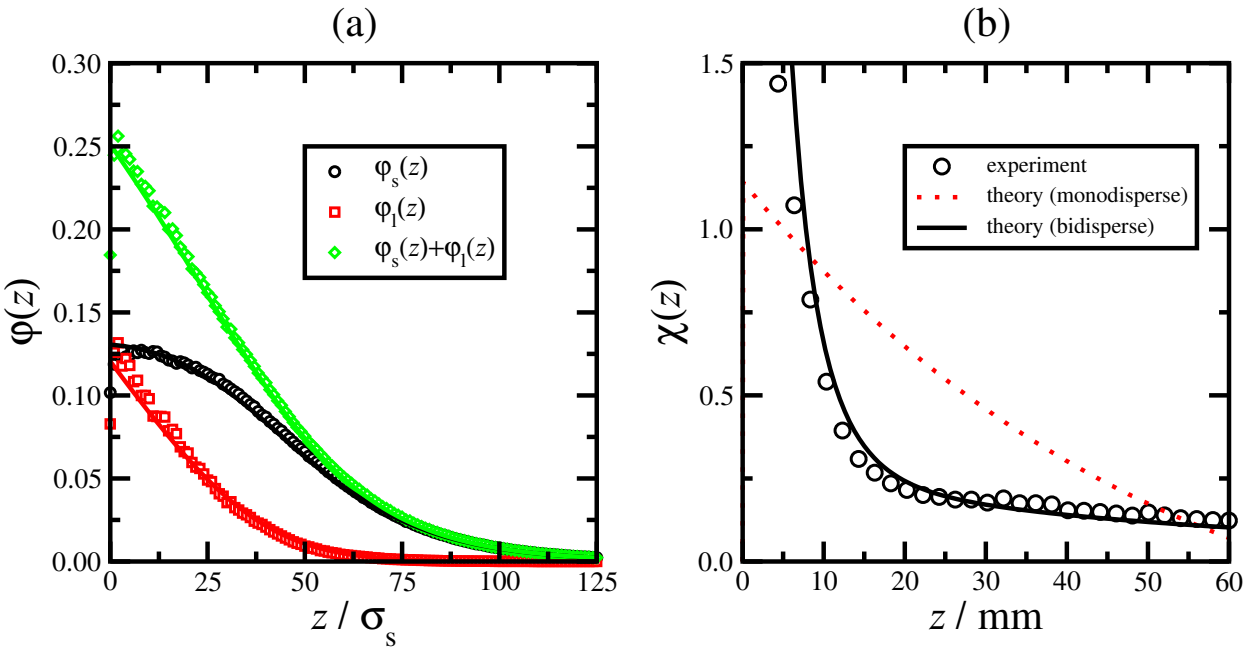

FIG. 6. (a) Volume-fraction profiles for small particles $\varphi_{\rm s}(z)$ and large particles $\varphi_{\rm l}(z)$, and the total volume-fraction profile $\varphi_{\rm s}(z)+\varphi_{\rm l}(z)$, in a bidisperse dipolar hard-sphere model – see text for parameters. The points are from Monte Carlo simulations and the lines are from theory. (b) Local susceptibility profile in a 60 mm section of a real polydisperse ferrofluid (points) with theoretical fits using a monodisperse model (dotted red line) and a bidisperse model (solid black line).

VIII. CONCLUSIONS

In this contribution, a very brief and necessarily selective survey is made of theoretical and computational work on the structural, magnetic, thermodynamic, and sedimentation properties of ferrofluids carried out as a collaboration between groups in Edinburgh and Ekaterinburg. In all cases, statistical-mechanical theory is combined with simple models of colloidal magnetic nanoparticles to give insights on the links between microscopic and macroscopic properties of fluids governed by strong dipole-dipole interactions. For well-defined models, simulations provide critical and well-controlled tests of theory. Favourable comparisons with experiments show that the models adopted provide faithful descriptions of reality.

Not only are the theoretical results applicable to ferrofluids, but with suitable extensions, they could apply to a broader class of molecular materials with electric dipole moments. The theoretical methods can also be applied to suspensions of magnetic particles with non-

spherical magnetic cores and/or anisotropic interactions [101], and this is a rapidly growing area in the field of magnetic fluids. Magnetic particles with rod-like [102], ellipsoidal [103], and even cubic [104] shapes can all be synthesised. The effective interactions between these types of particles are substantially different from those given by Eqs. 1–4, and are not so easily expressed. Nonetheless, computational studies on elongated magnetic particles [101] and magnetic cubes [105] predict highly non-trivial ground-state structures. Anisotropy in the short-range interactions can alter the ground-state conformations of particles at or close to contact. For example, elongating the hard core of a particle parallel to the dipole direction disfavours the nose-to-tail parallel conformation of two particles, and favours the side-by-side antiparallel ($\uparrow\downarrow$) arrangement [106]. Anisotropy can also be induced in spherical particles, where the distribution of magnetic material is non-uniform: examples include capped colloids [107] and magnetic Janus particles [108]. Clearly, there are many possibilities for making functional magnetic fluids, and there is plenty of work ahead to understand these fascinating materials.

ACKNOWLEDGMENTS

First and foremost, I would like to acknowledge the collaboration and friendship of the Ekaterinburg group, and in particular, Professors Alexey Ivanov, Ekaterina Elfimova, and Sofia Kantorovich. Their energy, enthusiasm, and expertise are boundless, and I'm fortunate to participate in their scientific programmes. Much of the work summarised herein was carried out – or at least initiated – during collaborative visits to Edinburgh and Ekaterinburg. Many of those visits were supported by the Ural Federal University, and their continued support of this work is gratefully acknowledged.

[1] R. E. Rosensweig, *Ferrohydrodynamics* (Dover Publications, Inc., New York, 1998).

[2] Q. A. Pankhurst, J. Connolly, S. K. Jones, and J. Dobson, J. Phys. D: Appl. Phys. **36**, R167 (2003).

[3] Q. A. Pankhurst, N. T. K. Thanh, S. K. Jones, and J. Dobson, J. Phys. D: Appl. Phys. **42**, 224001 (2009).

[4] P. I. C. Teixeira, J. M. Tavares, and M. M. Telo da Gama, J. Phys.: Condens. Matter **12**, R411 (2000).

[5] J. D. Jackson, *Classical Electrodynamics*, 3rd ed. (Wiley, New York, 1999).

[6] B. F. Edwards, D. M. Riffe, J.-Y. Ji, and W. A. Booth, Am. J. Phys. **85**, 130 (2017).

[7] W. H. Stockmayer, J. Chem. Phys. **9**, 398 (1941).

[8] I. Jacobs and C. Bean, Phys. Rev. **100**, 1060 (1955).

[9] T. Tlusty and S. A. Safran, Science **290**, 1328 (2000).

[10] A. Zilman, T. Tlusty, and S. A. Safran, J. Phys.: Condens. Matter **15**, S57 (2003).

[11] K. Butter, P. H. H. Bomans, P. M. Frederik, G. J. Vroege, and A. P. Philipse, Nature Materials **2**, 88 (2003).

[12] K. Butter, P. H. Bomans, P. M. Frederik, G. J. Vroege, and A. P. Philipse, J. Phys.: Condens. Matter **15**, S1451 (2003).

[13] M. Klokkenburg, R. P. A. Dullens, W. K. Kegel, B. H. Erné, and A. P. Philipse, Phys. Rev. Lett. **96**, 037203 (2006).

[14] M. Klokkenburg, B. H. Erné, J. D. Meeldijk, A. Wiedenmann, A. V. Petushkov, R. P. A. Dullens, and A. P. Philipse, Phys. Rev. Lett. **97**, 185702 (2006).

[15] J. J. Weis and D. Levesque, Phys. Rev. Lett. **71**, 2729 (1993).

[16] D. Levesque and J. J. Weis, Phys. Rev. E **49**, 5131 (1994).

[17] P. J. Camp and G. N. Patey, Phys. Rev. E **62**, 5403 (2000).

[18] L. Rovigatti, J. Russo, and F. Sciortino, Soft Matter **8**, 6310 (2012).

[19] D. Wei and G. N. Patey, Phys. Rev. Lett. **68**, 2043 (1992).

[20] D. Wei and G. N. Patey, Phys. Rev. A **46**, 7783 (1992).

[21] J. J. Weis and D. Levesque, Phys. Rev. E **48**, 3728 (1993).

[22] J.-J. Weis, J. Chem. Phys. **123**, 044503 (2005).

[23] J.-J. Weis and D. Levesque, J. Chem. Phys. **125**, 034504 (2006).

[24] M. A. Pounds and P. A. Madden, J. Chem. Phys. **126**, 104506 (2007).

[25] E. A. Elfimova, A. O. Ivanov, and P. J. Camp, J. Chem. Phys. **136**, 194502 (2012).

[26] Yu. E. Nekhoroshkova, O. A. Goldina, P. J. Camp, E. A. Elfimova, and A. O. Ivanov, J. Exp. Theor. Phys. **118**, 442 (2014).

[27] J.-P. Hansen and I. R. McDonald, *Theory of Simple Liquids*, 3rd ed. (Academic Press, London, 2006).

[28] D. J. Cebula, S. W. Charles, and J. Popplewell, Colloid. Polym. Sci. **259**, 395 (1981).

[29] F. Gazeau, E. Dubois, J.-C. Bacri, F. Boué, A. Cebers, and R. Perzynski, Phys. Rev. E **65**, 031403 (2002).

[30] G. Mériguet, F. Cousin, E. Dubois, F. Boué, A. Cebers, B. Farago, and R. Perzynski, J. Phys. Chem. B **110**, 4378 (2006).

[31] J. Wagner, B. Fischer, and T. Autenrieth, J. Chem. Phys. **124**, 114901 (2006).

[32] A. Wiedenmann, U. Keiderling, M. Meissner, D. Wallacher, R. Gähler, R. P. May, S. Preévost, M. Klokkenburg, B. H. Erné, and J. Kohlbrecher, Phys. Rev. B **77**, 184417 (2008).

[33] P. Langevin, J. Phys. Theor. Appl. **4**, 678 (1905).

[34] P. Weiss, J. Phys. Theor. Appl. **6**, 661 (1907).

[35] A. Tsebers, Magnetohydrodynamics **18**, 137 (1982).

[36] M. S. Wertheim, J. Chem. Phys. **55**, 4291 (1971).

[37] K. I. Morozov and A. V. Lebedev, J. Mag. Mag. Mater. **85**, 51 (1990).

[38] Yu. A. Buyevich and A. O. Ivanov, Physica A **190**, 276 (1992).

[39] A. O. Ivanov, Magnetohydrodynamics **28**, 353 (1992).

[40] A. F. Pshenichnikov, V. V. Mekhonoshin, and A. V. Lebedev, J. Mag. Mag. Mater. **161**, 94 (1996).

[41] A. O. Ivanov and O. B. Kuznetsova, Phys. Rev. E **64**, 041405 (2001).

[42] B. Huke and M. Lücke, Phys. Rev. E **62**, 6875 (2000).

[43] B. Huke and M. Lücke, Phys. Rev. E **67**, 051403 (2003).

[44] B. Huke and M. Lücke, Rep. Prog. Phys. **67**, 1731 (2004).

[45] I. Szalai and S. Dietrich, J. Phys.: Condens. Matter **20**, 204122 (2008).

[46] I. Szalai and S. Dietrich, J. Phys.: Condens. Matter **23**, 326004 (2011).

[47] I. Szalai, S. Nagy, and S. Dietrich, J. Phys.: Condens. Matter **25**, 465108 (2013).

[48] A. O. Ivanov, S. S. Kantorovich, E. N. Reznikov, C. Holm, A. F. Pshenichnikov, A. V. Lebedev, A. Chremos, and P. J. Camp, Phys. Rev. E **75**, 061405 (2007).

[49] A. O. Ivanov, S. S. Kantorovich, E. N. Reznikov, C. Holm, A. F. Pshenichnikov, A. V. Lebedev, A. Chremos, and P. J. Camp, Magnetohydrodynamics **43**, 393 (2007).

[50] J. O. Sindt, P. J. Camp, S. S. Kantorovich, E. A. Elfimova, and A. O. Ivanov, Phys. Rev. E **93**, 063117 (2016).

[51] P. J. Camp, E. A. Elfimova, and A. O. Ivanov, J. Phys.: Condens. Matter **26**, 456002 (2014).

[52] O. A. Goldina, A. V. Lebedev, A. O. Ivanov, and E. A. Elfimova, Magnetohydrodynamics **52**, 35 (2016).

[53] A. Y. Solovyova, O. A. Goldina, A. O. Ivanov, A. V. Lebedev, and E. A. Elfimova, J. Chem. Phys. **145**, 084909 (2016).

[54] S. Kantorovich, A. O. Ivanov, L. Rovigatti, J. M. Tavares, and F. Sciortino, Phys. Rev. Lett. **110**, 148306 (2013).

[55] H. Fröhlich, *Theory of dielectrics: dielectric constant and dielectric loss*, 2nd ed. (Clarendon Press, Oxford, 1987).

[56] U. M. Titulaer and J. M. Deutch, J. Chem. Phys. **60**, 1502 (1974).

[57] S. W. de Leeuw, J. W. Perram, and E. R. Smith, Proc. R. Soc. Lond. A **373**, 27 (1980).

[58] L. Onsager, J. Am. Chem. Soc. **58**, 1486 (1936).

[59] J. G. Kirkwood, J. Chem. Phys. **7**, 911 (1939).

[60] D. W. Jepsen, J. Chem. Phys. **44**, 774 (1966).

[61] A. D. Buckingham and C. G. Joslin, Mol. Phys. **40**, 1513 (1980).

[62] C. G. Joslin, Mol. Phys. **42**, 1507 (1981).

[63] C. Joslin and S. Goldman, Mol. Phys. **79**, 499 (1993).

[64] K. I. Morozov, J. Chem. Phys. **126**, 194506 (2007).

[65] R. E. Rosensweig, J. Magn. Magn. Mater. **252**, 370 (2002).

[66] R. Hergt, R. Hiergeist, I. Hilger, W. Kaiser, Y. Lapatnikov, S. Margel, and U. Richter, J. Magn. Magn. Mater. **270**, 345 (2004).

[67] F. Sonvico, S. Mornet, S. Vasseur, C. Dubernet, D. Jaillard, J. Degrouard, J. Hoebeke, E. Duguet, P. Colombo, and P. Couvreur, Bioconjug. Chem. **16**, 1181 (2005).

[68] J.-P. Fortin, C. Wilhelm, J. Servais, C. Ménager, J.-C. Bacri, and F. Gazeau, J. Am. Chem. Soc. **129**, 2628 (2007).

[69] W. F. Brown, Jr., J. Appl. Phys. **34**, 1319 (1963).

[70] W. F. Brown, Jr., IEEE Trans. Magn. **15**, 1196 (1979).

[71] A. O. Ivanov, V. S. Zverev, and S. S. Kantorovich, Soft Matter **12**, 3507 (2016).

[72] A. O. Ivanov, S. S. Kantorovich, E. A. Elfimova, V. S. Zverev, J. O. Sindt, and P. J. Camp, J. Mag. Magn. Mater. **431**, 141 (2017).

[73] A. O. Ivanov, S. S. Kantorovich, V. S. Zverev, E. A. Elfimova, A. V. Lebedev, and A. F. Pshenichnikov, Phys. Chem. Chem. Phys. **18**, 18342 (2016).

[74] E. A. Elfimova, A. O. Ivanov, and P. J. Camp, Phys. Rev. E **88**, 042310 (2013).

[75] E. A. Elfimova, A. O. Ivanov, and P. J. Camp, Phys. Rev. E **86**, 021126 (2012).

[76] K. Aim and I. Nezbeda, Fluid Phase Equil. **12**, 235 (1983).

[77] I. Nezbeda and W. R. Smith, Fluid Phase Equil. **216**, 183 (2004).

[78] J. Krejčí and I. Nezbeda, Fluid Phase Equil. **314**, 156 (2012).

[79] B. Luigjes, D. M. E. Thies-Weesie, A. P. Philipse, and B. H. Erné, J. Phys.: Condens. Matter **24**, 245103 (2012).

[80] B. Luigjes, D. M. E. Thies-Weesie, B. H. Erné, and A. P. Philipse, J. Phys.: Condens. Matter **24**, 245104 (2012).

[81] E. A. Elfimova, A. O. Ivanov, J. O. Sindt, and P. J. Camp, Mol. Phys. **113**, 3717 (2015).

[82] P. G. de Gennes and P. A. Pincus, Phys. Kondens. Materie **11**, 189 (1970).

[83] G. Stell, Phys. Rev. Lett. **32**, 286 (1974).

[84] M. E. van Leeuwen and B. Smit, Phys. Rev. Lett. **71**, 3991 (1993).

[85] J. O. Sindt and P. J. Camp, J. Chem. Phys. **143**, 024501 (2015).

[86] L. Rovigatti, J. Russo, and F. Sciortino, Phys. Rev. Lett. **107**, 237801 (2011).

[87] G. Ganzenmüller and P. J. Camp, J. Chem. Phys. **127**, 154504 (2007).

[88] N. G. Almarza, E. Lomba, C. Martín, and A. Gallardo, J. Chem. Phys. **129**, 234504 (2008).

[89] A. O. Ivanov, S. S. Kantorovich, and P. J. Camp, Phys. Rev. E **77**, 013501 (2008).

[90] Y. V. Kalyuzhnyi, I. A. Protsykevytch, G. Ganzenmüller, and P. J. Camp, Europhys. Lett. **84**, 26001 (2008).

[91] G. Ganzenmüller, G. N. Patey, and P. J. Camp, Mol. Phys. **107**, 403 (2009).

[92] R. P. Sear, Phys. Rev. Lett. **76**, 2310 (1996).

[93] R. van Roij, Phys. Rev. Lett. **76**, 3348 (1996).

[94] R. Piazza, S. Buzzaccaro, E. Secchi, and A. Parola, Soft Matter **8**, 7112 (2012).

[95] R. Piazza, S. Buzzaccaro, and E. Secchi, J. Phys.: Condens. Matter **24**, 284109 (2012).

[96] R. Piazza, Rep. Prog. Phys. **77**, 056602 (2014).

[97] A. F. Pshenichnikov, Instrum. Exp. Tech. **50**, 509 (2007).

[98] E. A. Elfimova, A. O. Ivanov, E. V. Lakhtina, A. F. Pshenichnikov, and P. J. Camp, Soft Matter **12**, 4103 (2016).

[99] A. O. Ivanov and S. S. Kantorovich, Phys. Rev. E **70**, 021401 (2004).

[100] E. Novak, E. Minina, E. Pyanzina, S. Kantorovich, and A. Ivanov, J. Chem. Phys. **139**, 224905 (2013).

[101] S. Kantorovich, E. Pyanzina, and F. Sciortino, Soft Matter **9**, 6594 (2013).

[102] T. Klein, A. Laptev, A. Günther, P. Bender, A. Tschöpe, and R. Birringer, J. Appl. Phys. **106**, 114301 (2009).

[103] S. Sacanna, L. Rossi, B. W. M. Kuipers, and A. P. Philipse, Langmuir **22**, 1822 (2006).

[104] L. Rossi, S. Sacanna, W. T. M. Irvine, P. M. Chaikin, D. J. Pine, and A. P. Philipse, Soft Matter **7**, 4139 (2011).

[105] J. G. Donaldson and S. S. Kantorovich, Nanoscale **7**, 3217 (2015).

[106] S. C. McGrother and G. Jackson, Phys. Rev. Lett. **76**, 4183 (1996).

[107] L. Baraban, D. Makarov, M. Albrecht, N. Rivier, P. Leiderer, and A. Erbe, Phys. Rev. E **77**, 031407 (2008).

[108] N. Zhao and M. Gao, Adv. Mater. **21**, 184 (2009).